Observation of the ballooning mode that limits the operation space of the high-density super-dense-core plasma in the LHD

S. Ohdachi[1,2], K. Y. Watanabe[1], K. Tanaka[1], Y. Suzuki[1, 2], Y. Takemura[1, 2], S. Sakakibara[1, 2], X. D. Du[1], T. Bando[2], Y. Narushima[1, 2], R. Sakamoto[1, 2], J. Miyazawa[1, 2], G. Motojima[1, 2], T. Morisaki[1, 2] and LHD Experiment Group[1]

[1]National Institute for Fusion Science, 322-6, Oroshi-cho, Toki, Japan
[2]SOKENDAI (The Graduate University for Advanced Studies), 322-6 Oroshi-cho, Toki, Japan

Corresponding Author: ohdachi@nifs.ac.jp

Abstract:
The central beta of the super–dense–core (SDC) plasma in the Large Helical Device (LHD) is limited by a large scale MHD event called "core density collapse" (CDC). The detailed measurement reveals that a new type of ballooning mode, quite localized in space and destabilized from the 3D nature of Heliotron devices, is the cause of the CDC. It is the first observation that the ballooning mode is excited where the global magnetic shear is negative. Avoidance of the excitation of this mode is a key to expand the operational limit of the LHD.

1 Introduction

High–density operation is one possible reactor scenario of helical confinement system. In the SDC type discharges [1], the electron density higher than 10^{21} m^{-3} with toroidal magnetic field $B_t = 2.5$ T is achieved in the LHD. It is much higher than the density in the equivalent Tokamak devices where the density limit is determined by the Greenwald limit. This is great advantage of the helical system. The SDC plasma is characterized by the fairly peaked density and pressure profiles. Fusion reactor with peaked density profile, similar to the SDC plasma, has many advantages. For example, since the fusion reaction rate is proportional to the density squared, the fusion reaction localized at the center of the plasma is anticipated.

However, when a steep pressure gradient is made, the large pressure gradient or the large boot–strap current density often drive MHD instabilities, for example in the edge localized mode [2] or the barrier localized mode [3]. The ballooning mode [4] is candidate

of MHD instability for the beta limit of the magnetically confined plasmas and can be destabilized in helical systems. The stability of the ballooning mode in helical systems is however more complicated than that in tokamaks. The rotational transform profile increases monotonically from the core to the edge ($0.4 \sim 1.4$, for example) in the vacuum magnetic field of Heliotron type devices. Since the current density is smaller in net–current free Heliotrons, the pressure profile mainly modifies the rotational transform profile. When the beta becomes large, from the Shafranov shift of the plasma, the rotational transform increases in the core region and decreases in the edge region. The rotational transform profile becomes flatter and is even reversed with a peaked pressure profile. There appears tokamak–like positive shear region in the core region. While tokamak–like ballooning modes within the positive shear region can be unstable for fairly high–beta condition, another kind of the ballooning mode is expected in the edge region where the magnetic shear remains negative [5, 6]. The stability of the ballooning mode is determined by the local magnetic properties, e.g., the local magnetic shear and the local magnetic curvature. The local magnetic shear $\hat{s_q}$ can be related to the global magnetic shear s_q [5, 6, 7],

$$\hat{s_q} = s_q - \alpha \mathcal{F} \cos\eta, \mathcal{F} = \begin{cases} 1. & \text{tokamak} \\ \frac{1+3s_q+\rho\beta''/\beta'}{4}. & \text{planer Heliotron} \end{cases} \quad (1)$$

, where $s_q = (\rho/q)(dq/d\rho)$, $\alpha = -R\beta' q^2 (> 0)$. R and ρ are the major and the averaged minor radius, respectively. η is the coordinate along the magnetic field line. q is the safety factor and the derivative denotes $d/d\rho$. In helical systems such as Helioton devices, it was pointed out that the local magnetic shear $\hat{s_q}$ becomes zero around the local pressure gradient peak ($\beta'' = 0$) with the large negative magnetic shear s_q. That is the reason why the ballooning mode can be unstable in helical system with a negative magnetic shear. The local magnetic curvature, which makes the ballooning mode unstable, is also different from that in tokamaks. In the low-beta condition, the magnetic curvature is mainly affected by the helicity. With the increase of the central beta, the magnetic axis shifted outward and the quite localized bad-curvature region formed in the low-magnetic field side of the torus due to the toroidicity. Therefore, this kind of high–mode–number–ballooning mode, referred to as the high–n ballooning mode, is caused by the three dimensional effect of the magnetic configurations and is different from the normal ballooning mode observed in Tokamaks.

In the SDC type experiments of the LHD, so-called core density collapse (CDC) events limit the increase of the central beta. In this article, from the measurements of the precursor oscillations observed before the CDC, the ballooning instability is considered to be the cause of this type of collapse. Though there is a report that the fast crashes observed in the Wendelstein 7–AS device might be caused by the ballooning mode [8], there was no clear evidence for the existence of the ballooning modes in the helical system. Therefore, this is the first report that the ballooning mode is destabilized in the helical system.

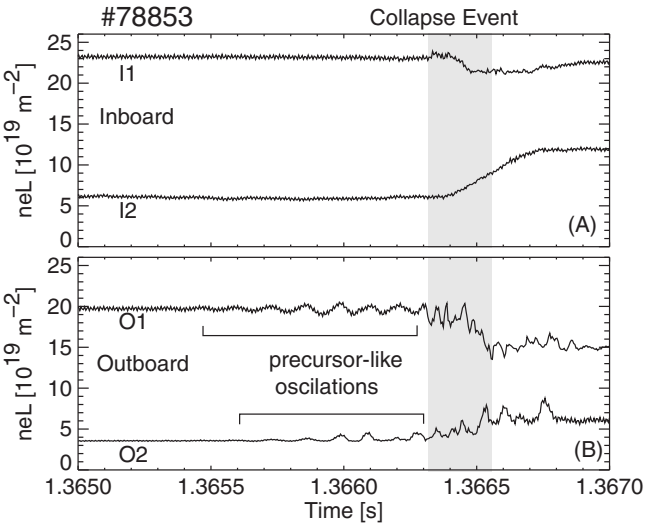

FIG. 1: Time evolution of the line averaged electron density measured by a CO_2 laser imaging interferometer measuring in the inboard side (A) and outboard side (B) is compared. The location of the each chord is shown as thick lines in Fig. 2 (C)

2 Precursor of the CDC

The Large Helical Device (LHD) is a planer Heliotron type device with the major radius $R = 3.9$m and the minor radius $a = 0.5\text{m} \sim 0.65$m [9]. A peaked pressure profile is formed during so-called super dense core (SDC) plasmas [1, 10] when the preset magnetic axis R_{ax0} is shifted outward ($R_{ax0} \geq 3.75m$). The SDC plasmas are made by the extensive central fueling by sequentially injected hydrogen pellets. While the density is slowly decreased after the pellet injection, the pressure or the beta profile is further peaked. The central beta reaches as high as 10%. The pressure gradient in this kind of discharges is one of the largest in LHD experiments. The limit of the profile peaking is determined by the collapse event called CDC [11, 12, 13]. The whole plasma is affected by this event; the central beta is decreased by 50% in the maximum case. Since the time scale of the event is very fast ($<$ 1ms), it is believed that this phenomenon is caused by MHD activities.

In the SDC plasmas, most of the advanced diagnostics for fluctuations in LHD do not work due to the high electron density. However, we can compare the fluctuations in the inboard side with those in the outboard side by an 80ch-CO_2 laser imaging interferometer system [14]. The chords cover almost whole plasma in a poloidal cross-section near one of the vertically elongated section (1.825° from the vertically elongated section toroidally). It is noted there are three groups of chords and there are two gaps between the chord groups as shown in Fig. 2(C). Time evolution of the line averaged electron density is shown in Fig. 1. Coherent oscillations with a frequency of about 8 kHz are observed at several hundreds of microseconds before the events only in the outboard side. Since the amplitude of the oscillations is increasing toward the collapse, it is quite likely that these oscillations are cause of the collapse.

The profile of the fluctuation level is shown in Fig. 2(B); the oscillations are localized

in the outboard side of the plasma. The spatial resolution of the measurement in the radial direction is about 6 mm. An extended view of the profile as a function of the averaged plasma minor radius ρ is shown in Fig. 2(B2).

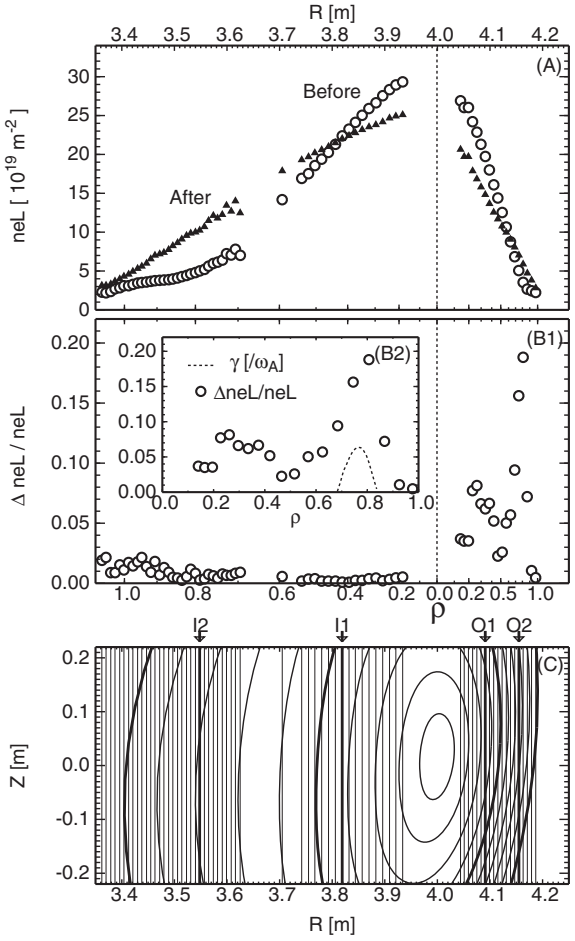

FIG. 2: The line-integrated density profile before / after CDC is shown in (A). The fluctuation levels as a function of the major radius (B1) and of the averaged minor radius in the outboard side (B2) are shown. ρ is defined from the outermost flux surface with which each chord interferes. The flux surfaces ($\rho = 0.1, 0.2, \ldots, 1.0$) and the location of the chords of the CO_2 laser interferometer are shown in (C). The dashed-line shown in (B2) is the growth rate of the ideal ballooning mode, which is as same as Fig. 3(D).

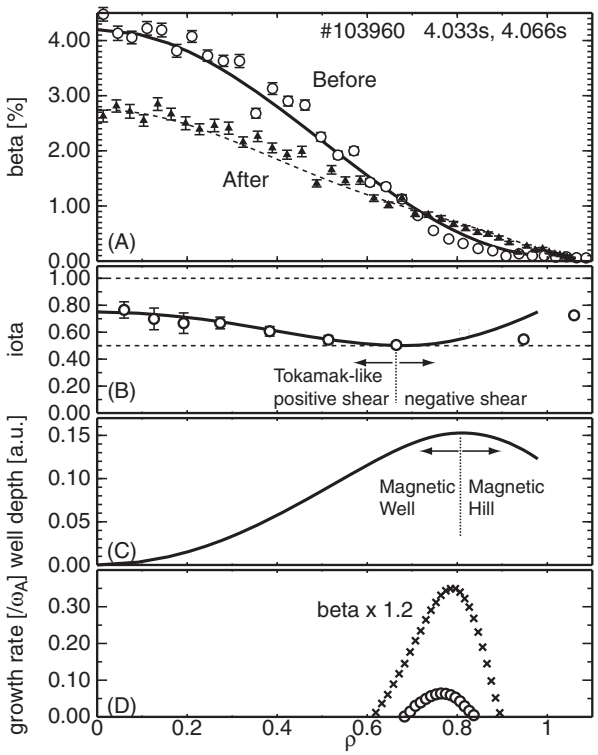

FIG. 3: Equilibrium profile just before the CDC is shown. The beta profile (just before the CDC (open circles) and after CDC (closed triangles)) measured by the Thomson scattering system (A), the rotational transform of VMEC equilibrium (solid line) and measured by MSE (open circles) (B), the magnetic well depth (C) and the growth rate of the ballooning mode calculated with the experimental pressure profile (open circles) and with the profile 1.2 times larger (crosses) (D) are shown together. In all plots, the effective minor radius r_{eff} of the each measuring position is determined first. ρ is then defined by the $\rho = r_{eff}/a_0$, where $a_0 (= 0.495m)$ is the averaged minor radius determined by the VMEC equilibrium.

These pre–cursor like oscillations are found in narrow regions. Note that, many positive

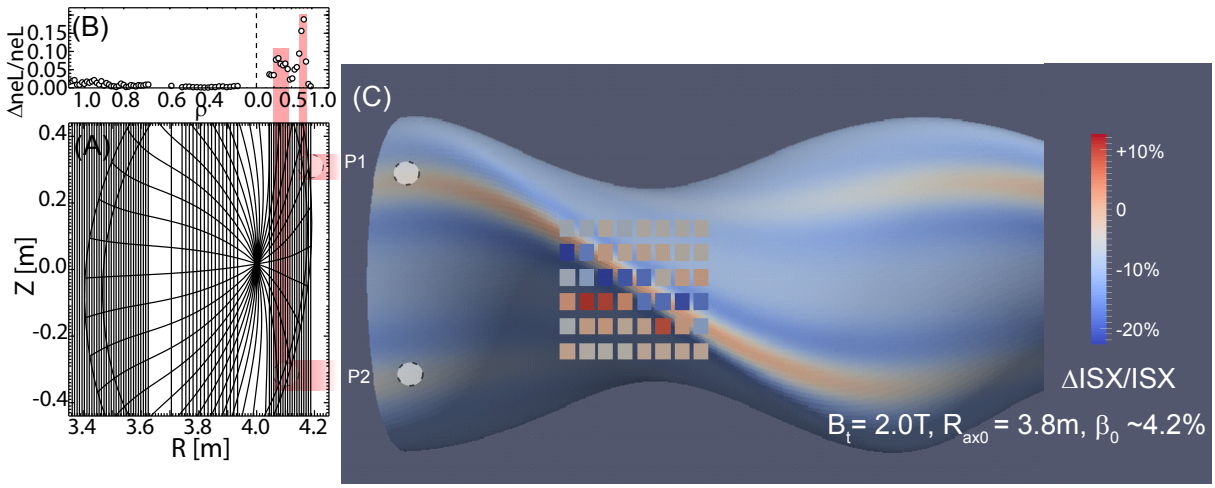

FIG. 4: Sightlines of CO_2 laser imaging interferometer (A), the line-integrated density fluctuation profile in the pre-cursor phase (B), hypothetical mode structure drawn on the surface of a 3D image of LHD plasma ($\rho \sim 0.8$) together with the 2D profile of the change in the SX emission just before the CDC (C) measured with 2D (6chx8ch) SX array. The magnitudes of the changes in SX are represented by color shown in the color bar. It is noted that the flux surface where the CO_2 laser imaging interferometer is slightly tilted.

spikes can be seen in the outer channels only in outboard side during / after the collapse. They might be parts of plasmas torn apart from the main plasma. Since this phenomena is observed only in the outboard side, the MHD activities seems to be also quite localized in the outboard side of the plasma

Figure 3 (A)–(C) shows the equilibrium calculated by the VMEC [15] code using the pressure profile (#103960 4033s) measured just before the CDC. The rotational transport profile is shown in Fig. 3(B). The experimentally measured profile (Fig. 3(B) circles) by the motional stark effect (MSE) system [16] agrees well with the calculated profile (solid line). There appears tokamak–like positive shear region in the core and the magnetic shear is still negative in the edge region, as stated in the introduction. From the profile of the magnetic well depth (Fig. 3(C)), the area with steep pressure gradient is within the magnetic well. This profile is therefore stable against the interchange mode. Low mode number MHD modes in the SDC plasmas have been shown to be stable from the stability analysis of the ideal MHD instabilities [17] as well. The growth rate of ideal high–n ballooning mode is calculated using a stability code Hn–bal [7]; the ballooning mode is locally unstable around $\rho \sim 0.8$ (Fig. 3(D)), which is consistent with the location of the precursor-like oscillations (Fig. 2(B2)). The growth rate increases rapidly with the increase in pressure profile ($\times$ 1.2 case is shown in Fig. 3(D)); this equilibrium is thus a boundary from stable to unstable. Since the magnetic shear is negative in that region, these instabilities should be the three-dimensional high–n ballooning mode.

There are two peaks in the fluctuation level profile in Fig. 2(B). If the mode structure of the pre-cursor is localized around a flux tube (See, 3D image of Fig. 4(C)) connected to the outboard side of the horizontally elongated section (worst curvature region), two

sharp peaks observed in the fluctuation profile shown in Fig. 4 (B) can be understood; two peaks correspond to mode structure observation at two location marked by closed white circles P1 and P2 in Fig. 4 (C). A newly developed 2D SX detector array [18] observing the bad curvature region shows that this pre-cursor like movement is aligned to the local magnetic field line (shown by color pixels in Fig. 4 (C)). This observation also supports that the mode structure is quite localized to the local magnetic field line.

In order to confirm the relation of the ballooning mode with the CDC phenomena further, stabilities with different magnetic configuration are investigated systematically. The stability of the ballooning mode is thus calculated assuming a fixed pressure profile, $p = p_0(1 - \rho^2)^2$ as a function of the preset magnetic axis R_{ax} [19]. When R_{ax} is shifted outward, the growth-rate of the ideal ballooning mode is larger with the same beta gradient (contour map in Fig. 5). The beta gradient observed just before the CDC is also shown with the open circles in Fig. 5. This tendency is qualitatively consistent with the observation that the CDC appears with a lower beta gradient when the preset magnetic axis is shifted outward. This fact also supports that the CDC is caused by the ideal high–n ballooning mode in the Helitron device.

Though the precursors are quite localized in space, the whole pressure profile is affected by the CDC phenomena as is shown in Fig. 3(A). It is quite different from the case of the edge localized mode observed in tokamaks. We are considering two scenarios to explain this. First one is the two–step scenario. At the beginning, the edge plasma is modified by the rapid growth of the ideal ballooning mode. The pressure gradient in the core region thereby becomes steeper further. This steeping triggers another MHD activity even in the core region with the magnetic well. It is consistent with the observation that in less collisional plasmas, large amplitude oscillations with the poloidal mode m = 1, which are not identified, is observed in the core instead of CDC [13]. Another idea is the ergodization of the magnetic field by the excitations of the edge ballooning mode. From the non-linear simulations, the enhanced radial flux caused by the ergodic magnetic field is expected after the evolution of the ballooning-like resistive mode [20].

3 Avoidance of the ballooning mode and beta limit

In order to avoid the CDC for achieving higher central beta, control of the ballooning mode by the reduction of the Shafranov-shift and by the reduction of the pressure gradient at the bad curvature region is experimentally performed. Plasma shape control using quadrupole magnetic field was effective to reduce the shift and controls the appearance of the CDC [21]. In the relatively low magnetic field experiment (B_t = 1.5 T), the pressure profile is broader than the profile with normal magnetic field B_t = 2.5 T (Fig. 6 (B)). It is consistent with the smaller growth rate predicted by Hn-Bal code with the smaller beta gradient as shown by the shaded area of Fig. 6 (B). The operational boundary observed in the 2.5 T can be passed over and the central beta has reached about 10% with B_t = 1.5 T and R_{ax0} = 3.75 m. It is the highest central beta achieved in the LHD and is comparable to the maximum central beta recorded in B_t = 0.45T experiments. Therefore, the mitigation of the high-n ballooning mode is proved to be the key to achieve high central beta in

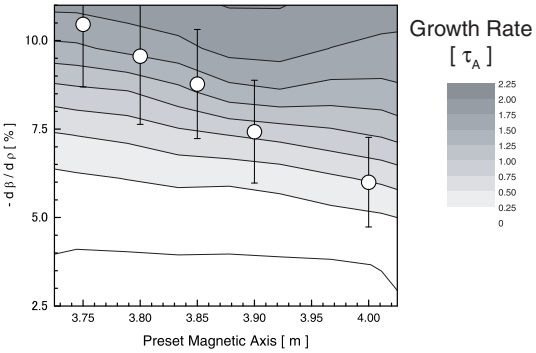

FIG. 5: The growth rate of the ideal ballooning mode as a function of the preset magnetic axis and the beta gradient at the beta gradient peak is shown. The beta gradient just before the CDC is shown with open circles at each preset magnetic axis positions. The y–error–bars denote the shot–by–shot variations.

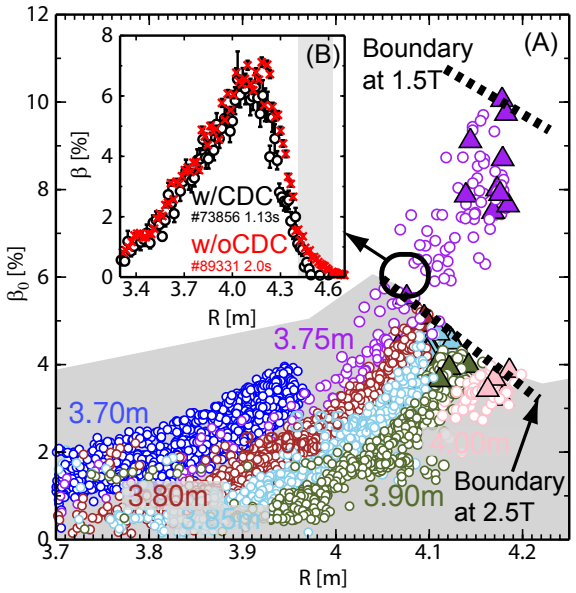

FIG. 6: The central beta as a function of the magnetic axis location is shown with different vacuum magnetic axis location Rax0. B_t = 2.5 T for R_{ax0} = 3.8-4.0 m and B_t = 1.5 T for R_{ax0} = 3.75 m. Triangle symbols indicate the appearance of the CDC. (B) Beta profile just before the CDC (2.5 T black) and without CDC (1.5 T: red) are shown. The parameter range is indicated by open ellipse in (A).

high-density SDC type operation of the LHD.

In summary, oscillations localized in the outboard side of the plasma just before the large-scale collapse event are found in a region with a negative magnetic shear. Since the profile is unstable against high-n ballooning mode and the location of the oscillations are consistent with the prediction by Hn–bal code, it should be the experimental evidence of the ballooning mode in the helical device.

Acknowledgement

This work was supported by NIFS budget code ULPP021, 028 and is also partially supported by the Ministry of Education, Science, Sports and Culture Grant-in-Aid for Scientific Research 26249144, by the JSPS-NRF-NSFC A3 Foresight Program (NSFC: No.11261140328, NRF: No. 2012K2A2A6000443), and by NIFS/NINS under the project of Formation of International Scientific Base and Network.

References

[1] N. Ohyabu, T. Morisaki, et. al., Physical review letters **97**, 55002 (2006).

[2] J. Connor, Plasma Physics and Controlled Fusion **40**,191 (1998).

[3] Y. Koide, et al., Plasma physics and controlled fusion **38**, 1011(1996).

[4] J. Connor, R. Hastie, and J. Taylor, Physical Review Letters **40**, 396 (1978).

[5] N. Nakajima, Physics of Plasmas **3**, 4545 (1996).

[6] N. Nakajima, Physics of Plasmas **3**, 4556 (1996).

[7] N. Nakajima, et. al., Fusionscience and technology **51**, 79 (2007).

[8] A. Weller, et al., Plasma Physics and Controlled Fusion **45**, A285 (2003).

[9] A. Komori, H. Yamada, et al., Fusion Science and Technology **58**, 1(2010).

[10] R. Sakamoto, H. Yamada, et. al. ., Fusion Science and Technology **58**, 53 (2010).

[11] H. Yamada, , Plasma Physics and Controlled Fusion **49**, B487 (2007).

[12] J. Miyazawa, R. Sakamoto, S. Ohdachi, et al., Plasma and Fusion Research **3**, 1047 (2008).

[13] S. Ohdachi, et al., Contributions to Plasma Physics **50**, 552 (2010).

[14] K. Tanaka, C. Michael, Plasma and Fusion Research **2**, 1033 (2007).

[15] S. P. Hirshman and P. van RIJ, Computer Physics Communications **43**, 143j (1986).

[16] K. Ida, Fusion Science and Technology **58**, 383 (2010).

[17] Y. Narushima, Journal of Plasma and Fusion Research Series **8**, 1070 (2009).

[18] Y. Takemura, S. Ohdachi, et. al., Rev. Sci. Instrum.**85**, 11E410 (2014)

[19] J. Varela, Plasma and Fusion Research **6**, 1403013 (2011).

[20] N. Mizuguchi, Y. Suzuki, and N. Ohyabu, Nuclear Fusion, **49**, 095023 (2009).

[21] J. Miyazawa, et. al., Plasma Fusion Res. **3**, S1047 (2008).